Proceedings of the CAS–CERN Accelerator School: Free Electron Lasers and Energy Recovery Linacs, Hamburg, Germany, 31 May–10 June 2016, edited by R. Bailey, CERN Yellow Reports: School Proceedings, Vol. 1/2018, CERN-2018-001-SP (CERN, Geneva, 2018)

Wakefields—An Overview

F. Reimann and U. van Rienen
University of Rostock, Rostock, Germany

Abstract
In this paper, we will report on the basic concepts of ultra-relativistic wakefields and their effects on particles while focusing; in this context, particularly on particle accelerators. We will introduce the commonly used terminology, and will derive and explain important quantities, such as the wake potential and wake function, the impedance as the Fourier transform of the wake potential, and loss parameters. To deepen knowledge on wake functions and potentials further, we will illustrate the derived quantities using, as examples, the cylindrical cavity and a rectangular waveguide lined with dielectrics.

Keywords
Wakefields; Green's functions; loss parameters; impedances.

1 Introduction

1.1 The term 'wakefield'

Outside of accelerator physics, the term 'wake' is mostly known from fluid dynamics, referring to the wave pattern behind an object moving in a liquid (e.g., a ship moving in water). This also comes to mind first if the term is used in everyday language.

In accelerator physics, the word 'wakefield' has a different meaning, as it describes an electromagnetic effect created by charged particles (see next paragraph). However, it is not completely wrong to think of the wakefield as a certain field pattern that follows a charged particle, as water waves follow a ship.

Wakefields, in the context of accelerator physics, are generated by a charged particle that travels through a metallic vacuum chamber. The self-field of an ultra-relativistic particle ends perpendicular to the highly conductive walls. On the surface of the walls, image charges are created (electric polarization), which turn into the sources of new fields and act back on the particle. In a metallic vacuum chamber without any geometric variation, the image charges travel together with the ultra-relativistic particle. Any geometric variation forces the field lines to bend, since they still need to stay perpendicular to the conductive walls. Then, some parts of the fields (and the energy stored therein) stay behind and consequently trail behind the particle. These fields are denoted wakefields. If a second particle follows the first closely enough, it will still see the wakefields of the first particle and interact with them. In a bunch of charged particles, the trailing particles of the bunch will see the wakefields of the leading particles and interact with them.

Figure 1 illustrates this process. A Gaussian pulse enters a so-called pillbox cavity. A pillbox cavity consists of a cylindrical cavity resonator with round openings that are attached to the beam pipe. The beam axis equals the symmetry axis of the pillbox cavity. At the transitions between the cylindrical cavity and the beam pipes, the diameter of the vacuum chamber changes so that a wakefield can be generated—a figurative description would say that part of the self-field of the bunch is 'stripped off' by the geometric changes in the structure. The wakefield remains in the structure and oscillates for some time after the bunch has left. A second particle bunch that traverses the structure would consequently be influenced by the generated wakefield. The pillbox cavity used in Fig. 1 has a radius of $R = 5\,\mathrm{cm}$ and a length of $R = 10\,\mathrm{cm}$ and will be used in examples throughout this paper as a model pillbox.

https://doi.org/10.23730/CYRSP-2018-001.125

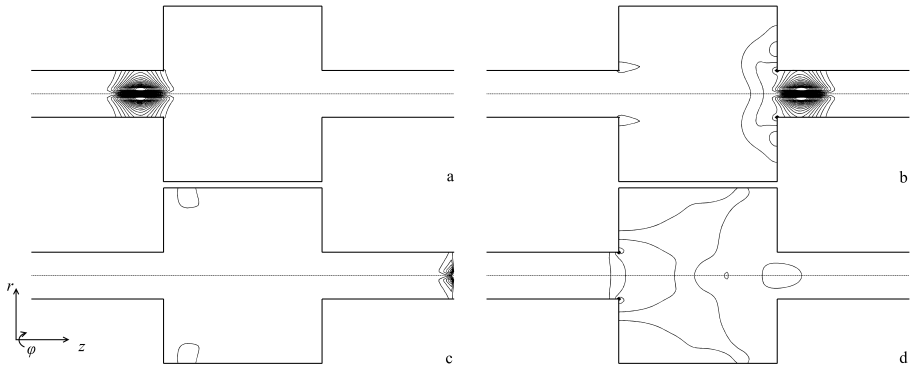

Fig. 1: Electric field lines of a Gaussian pulse travelling through the model pillbox cavity ($R = 5\,\mathrm{cm}, g = 10\,\mathrm{cm}$), calculated using the CST STUDIO SUITE® [1]: (a) while entering the structure; (b) leaving the cavity; (c) leaving the structure; (d) after leaving. It can be seen that a part of the electric field remains in the structure even after the bunch has left.

The word 'wakefield' is usually understood as a general term. More specifically, we speak about 'wake potentials', when considering the wakefield behind a particle bunch, and 'wake functions', when the wakefield behind a point charge is considered. These expressions will be explained in more detail in subsequent sections.

This report follows the lines of Ref. [2]. For further reading on wakefields and linear accelerators, please refer to Refs. [3–5].

1.2 Basic concepts of ultra-relativistic wakefields

To understand the underlying principles of wakefields, we first need to understand what happens to a point charge q that moves in free space with a velocity close to the speed of light, $v \approx c$.

Owing to the Lorentz contraction, the electromagnetic field of the electron will be shrunk to a thin disk perpendicular to its moving direction. The opening angle of the field travelling with the particle is given by $1/\sqrt{1-\beta^2} = 1/\gamma$ with the factor $\beta = v/c$. If the velocity approaches the speed of light, the thickness of the disk shrinks further, to a δ-distribution (see Fig. 2). This field is strictly radial, i.e., there are no components of the field *behind* or *in front* of the charge, which is also a consequence of the *principle of causality*. Accordingly, in this case, there can be no wakefield behind the electron in free space.

To actually achieve a field and a force behind the field-generating charge, additional mechanisms are required. For example, the image charges and fields created on the waveguide walls are only synchronous with the fields generating them if the walls are perfectly conducting. In resistive or imperfectly conducting walls, the image fields will trail behind the field-generating charge. Other possibilities include obstacles in the beam pipe, e.g., geometric variations (cf. Fig. 1), from which the fields are scattered. Another possibility is to introduce dielectric walls because the speed of light will be lower here than in a vacuum. This means that the fields are 'slowed down', in the sense that travelling waves in these media will have a lower phase velocity and thus trail behind the generating fields.

2 Basic definitions

In the following, we will consider a field-generating charge q_1, which is located at the three-dimensional coordinate $\mathbf{r}$. First, we want to examine the electromagnetic force that this field-generating charge exerts on a test charge q_2 that moves at the speed of light along the z-axis, $\mathbf{v} = c\mathbf{e}_z$. This force is simply the

Lorentz force,

$$\mathbf{F}\left(\mathbf{r},t\right)=q_2\left(\mathbf{E}\left(\mathbf{r},t\right)+c\mathbf{e}_z\times\mathbf{B}\left(\mathbf{r},t\right)\right)\,. \tag{1}$$

We introduce a new variable for the distance between q_2 and q_1 (see Fig. 3), so that

$$s=ct-z\,,$$

and

$$\mathbf{F}\left(s,t\right)=\mathbf{F}\left(x,y,z=ct-s,t\right).$$

The net momentum change δp of the test charge due to the Lorentz force will then be

$$\delta p\sim\int\mathbf{F}\left(s,t\right)\mathrm{d}t\,. \tag{2}$$

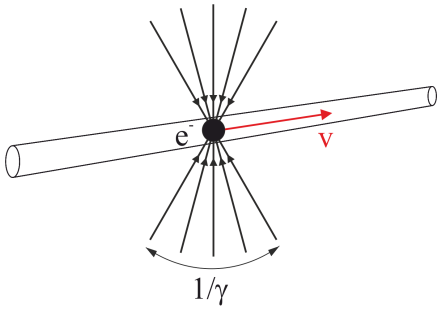

Fig. 2: Radial electric field of an electron moving at the speed of light, contracted to a disc.

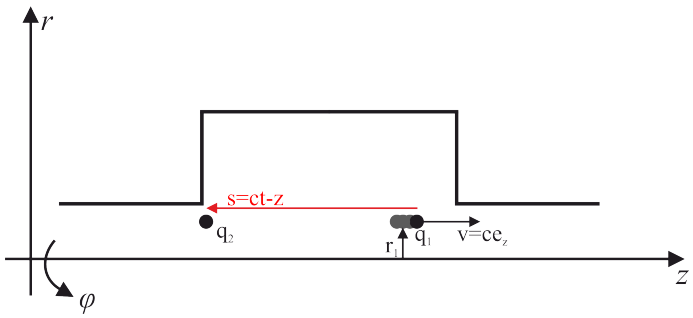

Fig. 3: Field-generating and test charges in a pillbox cavity. The grey dots represent the possibility of a particle bunch generating the wakefield instead of a single charge.

2.1 The wake potential

The concept of wake potentials is related to the concept of the momentum change on a test charge, described before. Consider the situation described in Fig. 3: a pillbox cavity with its transitions between the cylindrical cavity and the beam pipes introduces a radial change of the vacuum chamber and thus wakefields can be generated. Additionally, both charges are assumed to have a transverse offset $\mathbf{r}_1$ from the centre of the beam pipe, while the movement is still parallel to the z-axis. In cylindrical coordinates, the described situation is as shown in Fig. 3. For this case, the *three-dimensional wake potential* is defined as

$$\mathbf{W}\left(\mathbf{r}_1,s\right)=\frac{1}{q_1}\int\limits_{-\infty}^{\infty}\left[\mathbf{E}\left(\mathbf{r}_1,z,t\right)+c\mathbf{e}_z\times\mathbf{B}\left(\mathbf{r}_1,z,t\right)\right]_{t=(z+s)/c}\mathrm{d}z\,, \tag{3}$$

which is basically an integral over the Lorentz force evaluated on the beam axis and normalized to the field-generating charge. Additionally, time is substituted with $t=z+s/c$. The momentum change of the test charge is related to this via

$$\delta p=q_1q_2\mathbf{W}(s)\,. \tag{4}$$

Usually, the wake potential is separated into the *longitudinal wake potential* and the *transverse wake potential*.

For the longitudinal wake potential, the projection of the Lorentz force onto the z-axis is used:

$$\mathbf{W}\left(\mathbf{r}_1,s\right)\cdot\mathbf{e}_z=\frac{1}{q_1}\int\limits_{-\infty}^{\infty}\left[\mathbf{E}\left(\mathbf{r}_1,z,t\right)\cdot\mathbf{e}_z+c\left(\mathbf{e}_z\times\mathbf{B}\left(\mathbf{r}_1,z,t\right)\right)\cdot\mathbf{e}_z\right]_{t=(z+s)/c}\mathrm{d}z\,.$$

Here, the second term vanishes because $\mathbf{e}_z \cdot (\mathbf{e}_z \times \mathbf{B}(\mathbf{r}_1, z, t)) = 0$. The longitudinal component of the wake potential is thus only dependent on the electric field:

$$W_{||}(\mathbf{r}_1, s) = \frac{1}{q_1} \int_{-\infty}^{\infty} E_z \left(\mathbf{r}_1, z, \frac{z+s}{c} \right) \mathrm{d}z \,. \tag{5}$$

Consequently, the transverse wake potential is only dependent on the transverse components of the electric and magnetic field:

$$\mathbf{W}_{\perp}(\mathbf{r}_1, s) = \frac{1}{q_1} \int_{-\infty}^{\infty} \left[\mathbf{E}_{\perp}(\mathbf{r}_1, z, t) + c\mathbf{e}_z \times \mathbf{B}_{\perp}(\mathbf{r}_1, z, t) \right]_{t=(z+s)/c} \mathrm{d}z \,. \tag{6}$$

Both wake potentials are dependent on the distance s between the field-generating charges and the test charge. This distance is measured in the negative longitudinal direction (see Fig. 3). This means that a negative distance s corresponds to the case in which the test charge is *in front* of the field-generating charges. Owing to the principle of causality, in this case there can be *no wake potential*. Consequently, this means that:

$$W_{||}(\mathbf{r}_1, s) = 0 \text{ for } s < 0, \text{ and} \tag{7}$$

$$\mathbf{W}_{\perp}(\mathbf{r}_1, s) = 0 \text{ for } s < 0 \,. \tag{8}$$

Example wake potentials of Gaussian pulses inside a pillbox cavity are shown in Figs. 4 and 5.

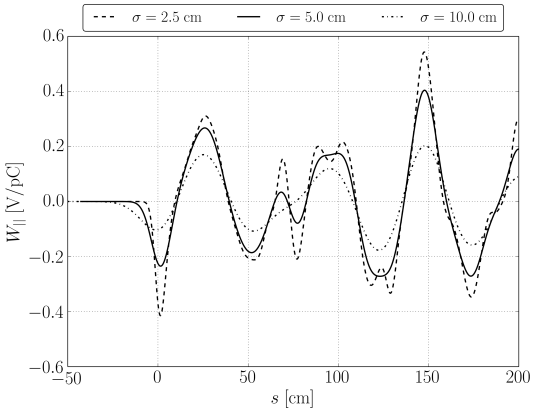

Fig. 4: Longitudinal wake potentials of Gaussian pulses with different pulse width σ inside the model pillbox cavity, computed using CST STUDIO SUITE ® [1].

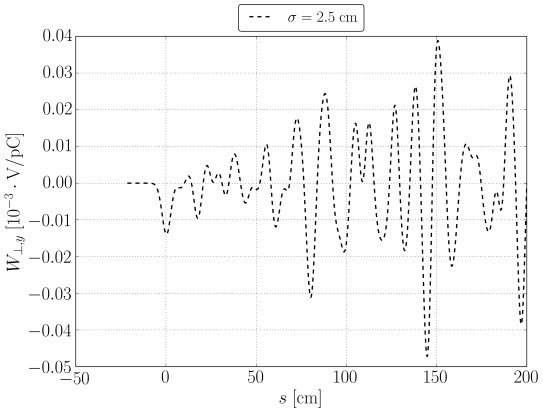

Fig. 5: Transverse wake potential of a Gaussian pulse of width $\sigma = 2.5$ cm inside the model pillbox cavity, computed using CST STUDIO SUITE ®. Note that the transverse wake potential is several orders of magnitude weaker than the longitudinal wake potential of the same pulse, displayed in Fig. 4.

2.2 The Panofsky–Wenzel theorem

The Panofsky–Wenzel theorem connects the longitudinal and transverse wake potentials via

$$\mathbf{W}_{\perp}(x, y, s) = -\nabla_{\perp} \int_{-\infty}^{s} \mathbf{W}_{||}\left(x, y, s'\right) \mathrm{d}s' \,. \tag{9}$$

Therefore, in principle, knowledge of only the longitudinal component of the wake potential is enough, since the transverse component can be constructed from it.

In the following, we want to briefly sketch the proof of this theorem.

We start with the transverse wake potential from Eq. (6). Its derivative with respect to s is

$$\frac{\partial}{\partial s}\mathbf{W}_\perp(\mathbf{r}_1,s)=\frac{1}{q_1}\int\limits_{-\infty}^{\infty}\Bigg[\underbrace{\frac{\partial}{c\partial t}\mathbf{E}_\perp(\mathbf{r}_1,z,t)}_{T_1}+\underbrace{\mathbf{e}_z\times\frac{\partial}{\partial t}\mathbf{B}_\perp(\mathbf{r}_1,z,t)}_{T_2}\Bigg]_{t=(z+s)/c}\mathrm{d}z\,, \tag{10}$$

where we used $s=ct-z$ and $\partial s=c\partial t$.

Now we want to replace T_1 and T_2 with more convenient expressions. For term T_1, we need the total derivative of the transverse electric field with respect to z. Using $s=ct-z$ this reads as

$$\frac{\mathrm{d}}{\mathrm{d}z}\mathbf{E}_\perp\left(\mathbf{r}_1,z,\frac{z+s}{c}\right)=\left(\frac{\partial}{\partial z}+\frac{1}{c}\frac{\partial}{\partial t}\right)\mathbf{E}_\perp\left(\mathbf{r}_1,z,\frac{z+s}{c}\right)\,,$$

where $\mathrm{d}/\mathrm{d}z$ is the total differential with respect to z. We reformulate T_1 in Eq. (10) as

$$\frac{1}{c}\frac{\partial}{\partial t}\mathbf{E}_\perp\left(\mathbf{r}_1,z,\frac{z+s}{c}\right)=\left(\frac{\mathrm{d}}{\mathrm{d}z}-\frac{\partial}{\partial z}\right)\mathbf{E}_\perp\left(\mathbf{r}_1,z,\frac{z+s}{c}\right)\,. \tag{11}$$

For term T_2, we start with Faraday's law of induction,

$$\nabla\times\mathbf{E}(\mathbf{r},t)=-\frac{\partial}{\partial t}\mathbf{B}(\mathbf{r},t)\,.$$

Computing the cross product of this equation with the beam axis leads to

$$\mathbf{e}_z\times\frac{\partial}{\partial t}\mathbf{B}(\mathbf{r},t)=-\mathbf{e}_z\times(\nabla\times\mathbf{E}(\mathbf{r},t))=\frac{\partial}{\partial z}\mathbf{E}_\perp(\mathbf{r},t)-\nabla_\perp E_z(\mathbf{r},t)\,. \tag{12}$$

Inserting Eqs. (11) and (12) into Eq. (10) results in

$$\begin{aligned}\frac{\partial}{\partial s}\mathbf{W}_\perp(\mathbf{r}_1,s)=\frac{1}{q_1}\int\limits_{-\infty}^{\infty}&\left(\frac{\mathrm{d}}{\mathrm{d}z}-\frac{\partial}{\partial z}\right)\mathbf{E}_\perp\left(\mathbf{r}_1,z,\frac{z+s}{c}\right)\\&+\left(\frac{\partial}{\partial z}\mathbf{E}_\perp\left(\mathbf{r}_1,z,\frac{z+s}{c}\right)-\nabla_\perp E_z\left(\mathbf{r}_1,z,\frac{z+s}{c}\right)\right)\mathrm{d}z\,.\end{aligned}$$

We reformulate this as

$$\frac{\partial}{\partial s}\mathbf{W}_\perp(\mathbf{r}_1,s)=\frac{1}{q_1}\int\limits_{-\infty}^{\infty}\frac{\mathrm{d}}{\mathrm{d}z}\mathbf{E}_\perp\left(\mathbf{r}_1,z,\frac{z+s}{c}\right)-\nabla_\perp\mathbf{E}_z\left(\mathbf{r}_1,z,\frac{z+s}{c}\right)\mathrm{d}z\,.$$

We assume perfect electric conductor boundary conditions at the waveguide walls so that the tangential electric field vanishes there. This simplifies Eq. (10) to

$$\frac{\partial}{\partial s}\mathbf{W}_\perp(\mathbf{r}_1,s)=-\frac{1}{q_1}\int\limits_{-\infty}^{\infty}\nabla_\perp\mathbf{E}_z\left(\mathbf{r}_1,z,\frac{z+s}{c}\right)\mathrm{d}z\,,$$

which is equivalent to

$$\frac{\partial}{\partial s}\mathbf{W}_\perp(\mathbf{r}_1,s)=-\nabla_\perp W_{||}(\mathbf{r}_1,s)\,.$$

Integrating the last statement over s leads to Eq. (9).

2.3 The fundamental theorem of beam loading

This section follows the lines of Ref. [5].

Up to this point, we only defined wakefields for $s > 0$. For $s < 0$, we concluded from the principle of causality that there can be no wakefield, and thus $\mathbf{W}(\mathbf{r}_1, s) = 0$.

We now want to consider the case of $s = 0$, which we had excluded before. For this, we will first look at a different example situation: two particles with equal charge q and a distance of a half wavelength, $\lambda/2$, between them are moving along the same axis, at the same speed. The first charge enters a previously empty cavity with no internal electric fields or stored energy (see Fig. 6). The charge will induce surface charges, electric fields, and voltages in the cavity,

$$V_i = -\int_C \mathbf{E}\,\mathrm{d}\mathbf{l}\,,$$

where the voltage is defined as a line integral over the electric field along a closed path C.

We will refer to this induced voltage as $-V_i$. This induced voltage is left in the cavity, even after the first charge left. From the law of energy conservation, we also infer that energy must be left behind in the cavity. However, the first charge will also 'see' a fraction a of its own induced voltage while in the cavity,

$$V_1 = -aV_i\,.$$

This corresponds to an energy loss of the first particle,

$$\Delta W_1 = qV_1 = -qaV_i\,.$$

Thus, with the first particle in the cavity, the net cavity voltage is $V_\mathrm{c} = -V_i$, while the stored energy U will be proportional to this voltage squared, $U \propto V_i^2$. This situation is shown in Fig. 7.

When the second particle arrives in the cavity, the voltage induced by the first particle will have changed phase by π, owing to the distance between the two particles. Thus, the induced voltage from particle 1 is now $+V_i$. The second particle, however, will *also* induce a voltage in the cavity of $-V_i$. The net cavity voltage will be

$$V_\mathrm{c} = +V_i - V_i = 0\,.$$

Particle 2 will also lose energy according to

$$\Delta W_2 = \underbrace{qV_i}_{\text{from particle 1}} - \underbrace{qaV_i}_{\text{from own induced voltage}}\,.$$

Since the net energy of the cavity must remain 0, the energy changes of particle 1 and 2 have to compensate each other (see Fig. 8),

$$\Delta W_1 + \Delta W_2 = 0\,,$$
$$qV_i - qaV_i - qaV_i = 0\,.$$

This leads directly to

$$a = \frac{1}{2}\,.$$

From this, we can directly derive the *fundamental theorem of beam loading*: a moving charge will experience (or 'see') half of its own induced voltage.

For the case of the wake potential, this implies that, for $s = 0$, when the field-generating and test charges are virtually at the same place, the wake potential must be multiplied by $1/2$. Thus, the final definition of the longitudinal wake potential is:

$$W_{||}(\mathbf{r}_1, s) = \frac{1}{q_1}\int_{-\infty}^{\infty} E_z\left(\mathbf{r}_1, z, \frac{z+s}{c}\right)\mathrm{d}z \begin{cases} 0 & \text{for } s < 0 \\ \frac{1}{2} & \text{for } s = 0 \\ 1 & \text{for } s > 0 \end{cases}. \tag{13}$$

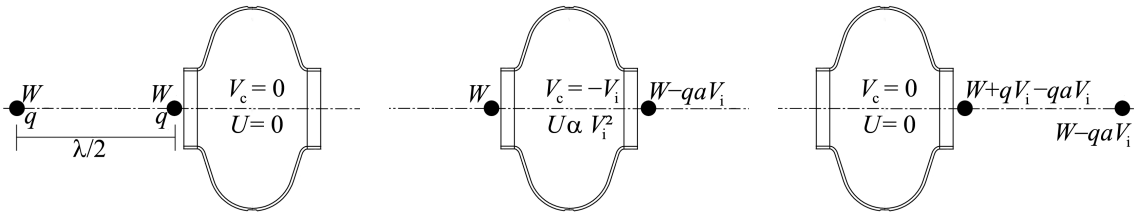

Fig. 6: Two charges separated by a distance $\lambda/2$ travelling along the same beam axis at the same speed are about to enter a previously empty elliptic cavity.

Fig. 7: The first charge has traversed the cavity and induced an image voltage of $-V_i$ in the cavity.

Fig. 8: Both charges have left the cavity. The total energy change in the cavity is 0, while both charges have lost energy, owing to the image fields they experienced. From this, the proportionality factor a can be calculated.

3 Impedances and loss parameters

3.1 Wakefields and impedances

The *impedance* is a physical quantity closely related to the wake potential by the Fourier transform:

$$Z_{||}\left(x,y,\omega\right) = \frac{1}{c}\int\limits_{-\infty}^{\infty} W_{||}\left(x,y,s\right)\exp\left(-\mathrm{i}\frac{\omega}{c}s\right)\mathrm{d}s\ . \tag{14}$$

Physically, the impedance and the wake potential describe one and the same effect; namely, the coupling between the beam and its environment. In contrast with the wake potential, which is described in the time domain, the impedance is described in the frequency domain. The impedance corresponds to a frequency spectrum that shows which of the structure's *eigenmodes* couple with the beam. The amplitude of the impedance in the frequency spectrum can also indicate the mode's coupling strength.

For more information on impedances, see Ref. [2].

3.2 Loss parameters

In the following, we want to have a closer look at the coupling strength of eigenmodes.

In general, it is possible to expand any physical quantity into a complete set of orthonormal functions. While in theory, *any* complete set of orthonormal functions will suffice, the choice of a suitable set of functions will usually decrease the effort for such an expansion while simultaneously increasing the numerical accuracy. For waveguide structures, the eigenmodes of the structure represent a suitable set of functions into which other fields can be expanded, e.g., the electric and magnetic field. This is often done if a straightforward solution of Maxwell's equation to obtain these fields directly is either very difficult or outright impossible.

In this case, let us assume that we expand the electric field inside an arbitrary cavity or waveguide into a set of this structure's spatial eigenmodes $\mathbf{E}_n\left(\mathbf{r}\right)$,

$$\mathbf{E}\left(\mathbf{r},t\right) = \sum_{n=0}^{\infty}\chi_n\left(t\right)\mathbf{E}_n\left(\mathbf{r}\right)\ . \tag{15}$$

This expansion is analytically correct as long as the upper limit of the summation is infinity. Of course, this is not feasible for practical use. For the moment, however, it shall be sufficient to note that if the summation is ceased after a finite number of terms, the expansion will be a mere *approximation* of the

analytically correct result, and that the quality of the approximation strongly depends on the number of expansion functions used.

From the spatial electric fields, the energy stored in each of these eigenmodes can be computed according to

$$U_n = \frac{\epsilon_0}{2} \int |\mathbf{E}_n(\mathbf{r})|^2 \, \mathrm{d}^3 r \, . \tag{16}$$

A point charge moving at c along the beam axis will experience a voltage drop (per mode) of

$$V_n = \int_{-\infty}^{\infty} E_{z,n}(z) \exp\left(\mathrm{i}\frac{\omega_n z}{c}\right) \mathrm{d}z, \tag{17}$$

where ω_n is the eigenfrequency of the mode.

The *loss parameter* k_n of an eigenmode is defined using these two quantities,

$$k_n = \frac{|V_n|^2}{4U_n} \, . \tag{18}$$

It is independent of the phase and frequency of the eigenmode and represents the eigenmode's coupling strength to the beam and thus its contribution to the wakefield. Moreover, it describes how much energy a point charge loses into a mode n by

$$\Delta W_n = q_1^2 k_n \, .$$

Another useful aspect of the loss parameters is that they are closely related to the wakefield of a point charge (called the *wake function*),

$$W_{||,0} = \sum_{n=0}^{\infty} 2k_n \cos\left(\frac{\omega_n s}{c}\right) \begin{cases} 0 & \text{for } s < 0 \\ \frac{1}{2} & \text{for } s = 0 \\ 1 & \text{for } s > 0 \end{cases} . \tag{19}$$

The wake function is a sum of the contributions from all modes, and can be calculated from just the knowledge of the loss parameters and the eigenfrequencies of the modes. Its main merit is that it serves as a *Green's function*, i.e., the wake potentials of any arbitrary bunch shape can be derived from it by convolution.

We assume a bunch with the shape function $\psi(s)$, i.e., a normalized distribution of particles measured relative to the field-generating particle. This bunch's wake potential can be obtained from the wake function via a convolution with the bunch shape function,

$$W_{||}(s) = \int_0^{\infty} \psi\left(s - s'\right) W_{||,0}\left(s'\right) \mathrm{d}s' \, . \tag{20}$$

This relation makes the wake function a very versatile quantity. For simple geometries, it is possible to calculate the eigenmodes, and thus the wake function, analytically. In general, there exist several error sources, owing to the different kinds of approximation needed. First, there is truncation error in the series expansion. Second, for customary accelerating cavities, it is usually necessary to compute the eigenmodes numerically, thus introducing a numerical error. This can render the numerical determination of the wake function infeasible in a number of cases. However, numerical software, as e.g., CST STUDIO SUITE®, is able to compute the wake potential but not the wake function, as this would require modelling of the idealized point charge. Such software directly computes the wake potential of the studied bunch shape. Should the wake function be needed and not be available analytically, it is then often replaced with the wake potential of a very short Gaussian bunch (since an infinitesimally short Gaussian pulse would represent a point charge). Again, this is an approximation and can lead to systematic errors.

Another quantity related to the wake potential and the bunch shape function is the total loss parameter of the bunch,

$$k_{\mathrm{tot}} = \int_{-\infty}^{\infty} \psi\left(s\right) W_{||}\left(s\right) \mathrm{d}s\,. \tag{21}$$

The total loss parameter can give information about the total power lost due to wake potential, P_{tot} via

$$P_{\mathrm{tot}} = I q k_{\mathrm{tot}}\,, \tag{22}$$

where I denotes the electric current.

4 Example 1: cylindrical cavity

4.1 The eigenmodes

In this section, we want to examine the longitudinal wake potential inside a cylindrical cavity. We assume that the cavity has a radius of R and a width of g, and that all the cavity walls are perfectly conducting. For the sake of simplicity, we also assume that the point charge traverses the cavity on the z-axis so that $\mathbf{r}_1 = \mathbf{0}$.

A pillbox cavity with beam pipes, as shown in Fig. 3, could also be regarded as such a cylindrical structure below the cut-off frequencies of the interesting eigenmodes (a length of the beam pipes above the attenuation length of these modes). For the rest of this subsection, though, we will restrict our considerations to the ideal cylindrical cavity.

First, we regard the eigenmodes of the evacuated cavity. For this example, it is possible to obtain an analytical expression for the eigenmodes by solving Maxwell's equations inside the cavity (for a harmonic time dependence, $\rho = 0$ and $\mathbf{j} = \mathbf{0}$):

$$\nabla \cdot \mathbf{E}\left(\mathbf{r}\right) = 0\,, \tag{23}$$

$$\nabla \cdot \mathbf{B}\left(\mathbf{r}\right) = 0\,, \tag{24}$$

$$\nabla \times \mathbf{E}\left(\mathbf{r}\right) = -\mathrm{i}\omega \mathbf{B}\left(\mathbf{r}\right)\,, \tag{25}$$

$$\nabla \times \mathbf{B}\left(\mathbf{r}\right) = \mathrm{i}\frac{\omega}{c^2} \mathbf{E}\left(\mathbf{r}\right)\,. \tag{26}$$

Generally, two types of eigenmode can exist in cavities. *Transverse electric (TE)* modes do not exhibit an electric field component in the longitudinal direction (in most cases, this means $E_z = 0$); for *transverse magnetic (TM)* modes the magnetic field is zero in the longitudinal direction ($B_z = 0$). (The third type, the *transverse electromagnetic (TEM)* mode, cannot exist in a cylindrical cavity. Its occurrences are limited to geometries in which two isolated conductors exist, such as in coaxial cables, or to mode considerations in structures that are not electrically conducting.) Since we want to determine the longitudinal wakefield, which is an integral over the longitudinal electric field according to Eq. (5), we do not need to consider TE modes for this purpose, since their electric field along the z-axis is zero. Therefore, we will restrict our consideration to TM modes.

Choosing a vector potential $\mathbf{A}(\mathbf{r})$ and defining the magnetic field as its rotation,

$$\mathbf{B}(\mathbf{r}) = \nabla \times \mathbf{A}(\mathbf{r})\,, \tag{27}$$

automatically fulfils Eq. (24), since $\nabla \cdot \mathbf{B} = \nabla \cdot (\nabla \times \mathbf{A}) = 0$. Additionally, since for all TM modes $B_z = 0$, it is convenient to choose the vector potential parallel to the z-axis:

$$\mathbf{A}(\mathbf{r}) = A(\mathbf{r})\, \mathbf{e}_z\,. \tag{28}$$

In this way, Eq. (27) automatically results in a magnetic field with $B_z = 0$.

The dependence of the electric field on the vector potential can be determined by plugging Eq. (27) into Eq. (25),

$$\nabla \times \mathbf{E}\left(\mathbf{r}\right) = -\mathrm{i}\omega \nabla \times \mathbf{A}\left(\mathbf{r}\right) .$$

This means that, up to the gradient of a scalar potential ϕ, the electric field and the vector potential are equivalent,

$$\mathbf{E}\left(\mathbf{r}\right) = -\mathrm{i}\omega \left(\mathbf{A}\left(\mathbf{r}\right) + \nabla\phi\right) . \tag{29}$$

Inserting Eq. (27) into Eq. (26), and using fundamental vector algebra, yields:

$$\nabla \times \nabla \times \mathbf{A}\left(\mathbf{r}\right) = \nabla \cdot \left(\nabla \cdot \mathbf{A}\left(\mathbf{r}\right)\right) - \nabla^2 \mathbf{A}\left(\mathbf{r}\right) = \mathrm{i}\frac{\omega}{c^2}\mathbf{E}\left(\mathbf{r}\right) .$$

After we insert Eq. (29) into this equation, we can choose the gauge $\phi = \frac{c^2}{\omega^2}\nabla \cdot \mathbf{A}$,

$$\begin{aligned}\nabla \cdot \left(\nabla \cdot \mathbf{A}\left(\mathbf{r}\right)\right) - \nabla^2 \mathbf{A}\left(\mathbf{r}\right) &= \frac{\omega^2}{c^2}\left(\mathbf{A}\left(\mathbf{r}\right) + \nabla\phi\right) \\ &= \frac{\omega^2}{c^2}\mathbf{A}\left(\mathbf{r}\right) - \frac{\omega^2}{c^2}\nabla \cdot \left(\frac{c^2}{\omega^2}\nabla \cdot \mathbf{A}\left(\mathbf{r}\right)\right) ,\end{aligned}$$

and eliminate two terms.

Introducing the wavenumber $k^2 = \omega^2/c^2$, this leads to the Helmholtz equation for the vector potential,

$$\nabla^2 \mathbf{A}\left(\mathbf{r}\right) + k^2 \mathbf{A}\left(\mathbf{r}\right) = 0 . \tag{30}$$

Since we chose the vector potential to be parallel to the z-axis and the Laplacian is a scalar operator, we can simplify this equation to

$$\nabla^2 A\left(\mathbf{r}\right) + k^2 A\left(\mathbf{r}\right) = 0 .$$

It is convenient to work in cylindrical coordinates in this case. In cylindrical coordinates, the Helmholtz equation reads

$$\frac{1}{r}\frac{\partial}{\partial r}\left(r\frac{\partial}{\partial r}\right) A\left(r,\varphi,z\right) + \frac{1}{r^2}\frac{\partial^2}{\partial \varphi^2} A\left(r,\varphi,z\right) + \frac{\partial^2}{\partial z^2} A\left(r,\varphi,z\right) = -k^2 A\left(r,\varphi,z\right) . \tag{31}$$

To solve this equation, we employ a separation ansatz for A. We assume that $A\left(r,\varphi,z\right) = A_r\left(r\right) A_\varphi\left(\varphi\right) A_z\left(z\right)$. Using this ansatz and dividing by $A\left(r,\varphi,z\right)$ leads to three separate equations:

$$\frac{1}{r}\frac{\partial}{\partial r}\left(r\frac{\partial}{\partial r}\right) A_r\left(r\right) = -k_r^2 A_r\left(r\right) , \tag{32}$$

$$\frac{1}{r^2}\frac{\partial^2}{\partial \varphi^2} A_\varphi\left(\varphi\right) = -k_\varphi^2 A_\varphi\left(\varphi\right) , \tag{33}$$

$$\frac{\partial^2}{\partial z^2} A_z\left(z\right) = -k_z^2 A_z\left(z\right) , \tag{34}$$

together with the separation equation $k^2 = k_r^2 + k_\varphi^2 + k_z^2$.

The solution of Eq. (34) can be expressed generally as a linear combination of sine and cosine functions,

$$A_z\left(z\right) = C_{z,1}\sin\left(k_z z\right) + C_{z,2}\cos\left(k_z z\right) . \tag{35}$$

For the solution of Eq. (33), we want to reformulate the equation first,

$$\frac{\partial^2}{\partial \varphi^2} A_\varphi\left(\varphi\right) = -\underbrace{k_\varphi^2 r^2}_{=m^2} A_\varphi\left(\varphi\right) .$$

The solution of this equation, like the solution of A_z, can be expressed as a linear combination of sine and cosine functions. Moreover, because of the periodicity of the structure regarding the angle φ, the condition $A_\varphi(\varphi) = A_\varphi(\varphi + 2\pi)$ must be met. From this, we can deduce that m has to be an integer. Without any loss of generality, the origin can always be set such that either a sine or a cosine function is sufficient to express A_φ. Since the sine function would be zero for $m = 0$, we choose the cosine, so that

$$A_\varphi(\varphi) = C_\varphi \cos(m\varphi) \ , \text{ with } m = 0, 1, 2, 3 \ldots \tag{36}$$

With these two solutions at hand, we now examine the radial equation, Eq. (32). Using the separation equation to replace k_r, it can be reformulated as

$$\frac{1}{r}\frac{\partial}{\partial r}A_r(r) + \frac{\partial^2}{\partial r^2}A_r(r) = -\left(k^2 - k_z^2 - k_\varphi^2\right)A_r(r) \ .$$

We now multiply the whole equation with r^2 and substitute $k_\varphi^2 = m^2/r^2$, so that

$$r^2\frac{\partial^2}{\partial r^2}A_r(r) + r\frac{\partial}{\partial r}A_r(r) = -r^2\left(k^2 - k_z^2 - \frac{m^2}{r^2}\right)A_r(r) \ . \tag{37}$$

The solutions of this equation are the so-called *Bessel functions* Z_m. Accordingly, the solution can be written as

$$A_r(r) = Z_m\left(r\sqrt{k^2 - k_z^2}\right) \ .$$

For a restricted area, like the cylindrical cavity, only the Bessel functions of the first kind, J_m, and the Bessel functions of the second kind, Y_m, must be considered. Since the functions of the second kind diverge for $r \to 0$, we can restrict the solution to the functions of the first kind,

$$A_r(r) = J_m(Kr) \ , \tag{38}$$

where we introduce $K = \sqrt{k^2 - k_z^2}$.

The complete solution for the vector potential $\mathbf{A}(r)$ is a product of Eqs. (38), (36), and (35):

$$\mathbf{A}(r, \varphi, z) = C_\varphi J_m(Kr)\cos(m\varphi)\left(C_{z,1}\sin(k_z z) + C_{z,2}\cos(k_z z)\right)\mathbf{e}_z \ . \tag{39}$$

The resulting components of the electric and magnetic field can be determined by employing the curl in cylindrical coordinates and using Eqs. (27), (26), and (29):

$$\begin{aligned}
B_r(r, \varphi, z) &= \frac{1}{r}\frac{\partial}{\partial \varphi}A = -C_\varphi\frac{m}{r}J_m(Kr)\sin(m\varphi)\left(C_{z,1}\sin(k_z z) + C_{z,2}\cos(k_z z)\right) \ , \\
B_\varphi(r, \varphi, z) &= -\frac{\partial}{\partial r}A = -C_\varphi K J_m'(Kr)\cos(m\varphi)\left(C_{z,1}\sin(k_z z) + C_{z,2}\cos(k_z z)\right) \ , \\
E_r(r, \varphi, z) &= \mathrm{i}\frac{c^2}{\omega}\frac{\partial}{\partial z}B_\varphi = \mathrm{i}C_\varphi\frac{k_z c^2}{\omega}K J_m'(Kr)\cos(m\varphi)\left(C_{z,1}\cos(k_z z) - C_{z,2}\sin(k_z z)\right) \ , \\
E_\varphi(r, \varphi, z) &= -\mathrm{i}\frac{c^2}{\omega}\frac{\partial}{\partial z}B_r = -\mathrm{i}C_\varphi\frac{k_z c^2}{\omega}\frac{m}{r}J_m(Kr)\sin(m\varphi)\left(C_{z,1}\cos(k_z z) - C_{z,2}\sin(k_z z)\right) \ , \\
E_z(r, \varphi, z) &= -\mathrm{i}\frac{c^2}{\omega}K^2 A = -\mathrm{i}C_\varphi\frac{c^2}{\omega}K^2 J_m(Kr)\cos(m\varphi)\left(C_{z,1}\sin(k_z z) + C_{z,2}\cos(k_z z)\right) \ ,
\end{aligned}$$

where we introduce the derivative of the Bessel function,

$$J_m' = \frac{\mathrm{d}}{\mathrm{d}(Kr)}J_m(Kr) \ .$$

To specify this intermediate solution, we also need to employ boundary conditions. We assumed that the cavity is made of perfect electric conductor material, so that the tangential electric field components vanish at the boundaries. In the radial direction, this means that E_z and E_φ must be zero at the boundary at $r = R$. Both components are proportional to J_m, so that we can deduce

$$J_m\left(Kr\right) = 0\,,\ \text{at } r = R\,.$$

From this we can determine the eigenvalue K with

$$K = \frac{j_{m,n}}{R}\,, \tag{40}$$

with $j_{m,n}$ referring to the nth zero of the Bessel function J_m.

In the longitudinal direction, the perfect electric conductor condition means that E_r and E_φ must be zero at the boundaries at $z = 0$ and $z = g$. Both components are proportional to the derivative of A_z. From this, we can deduce that:

$$\frac{\mathrm{d}}{\mathrm{d}z}A_z\left(z\right)\bigg|_{z=0,z=g} = k_z\left(C_{z,1}\cos\left(k_z z\right) - C_{z,2}\sin\left(k_z z\right)\right)\big|_{z=0,z=g} = 0\,.$$

For $z = 0$, the sine term always vanishes. To meet the boundary condition, the cosine term must also vanish, which can only be fulfilled if $C_{z,1} = 0$. The second condition thus simplifies to

$$-k_z C_{z,2}\sin\left(k_z g\right) = 0\,,$$

which is fulfilled for $k_z = p\pi/g$ and integer mode numbers p.

With these specifications the field components can be finalized as:

$$\begin{aligned}
B_r^{m,n,p}\left(r,\varphi,z\right) &= -C\frac{m}{r}J_m\left(j_{m,n}\frac{r}{R}\right)\sin\left(m\varphi\right)\cos\left(p\pi\frac{z}{g}\right)\,,\\
B_\varphi^{m,n,p}\left(r,\varphi,z\right) &= -C\frac{j_{m,n}}{R}J_m'\left(j_{m,n}\frac{r}{R}\right)\cos\left(m\varphi\right)\cos\left(p\pi\frac{z}{g}\right)\,,\\
E_r^{m,n,p}\left(r,\varphi,z\right) &= -\mathrm{i}C\frac{p\pi}{g}\frac{c^2}{\omega_{m,n,p}}\frac{j_{m,n}}{R}J_m'\left(j_{m,n}\frac{r}{R}\right)\cos\left(m\varphi\right)\sin\left(p\pi\frac{z}{g}\right)\,,\\
E_\varphi^{m,n,p}\left(r,\varphi,z\right) &= \mathrm{i}C\frac{p\pi}{g}\frac{c^2}{\omega_{m,n,p}}\frac{m}{r}J_m\left(j_{m,n}\frac{r}{R}\right)\sin\left(m\varphi\right)\sin\left(p\pi\frac{z}{g}\right)\,,\\
E_z^{m,n,p}\left(r,\varphi,z\right) &= -\mathrm{i}C\frac{c^2}{\omega_{m,n,p}}\left(\frac{j_{m,n}}{R}\right)^2 J_m\left(j_{m,n}\frac{r}{R}\right)\cos\left(m\varphi\right)\cos\left(p\pi\frac{z}{g}\right)\,,
\end{aligned} \tag{41}$$

with the integer mode numbers m, n, and p and the normalization constant $C = C_\varphi C_{z,2}$. The eigenfrequency of the modes is

$$\omega_{m,n,p} = \sqrt{\left(\frac{j_{m,n}}{R}\right)^2 + \left(\frac{p\pi}{g}\right)^2}\,. \tag{42}$$

For more information on the eigenmodes of cylindrical structures, see Ref. [6].

4.2 The loss parameters and the monopole wake function

We want to further limit our considerations to the so-called monopole modes, and the subsequent monopole wake function. In the monopole case, the azimuthal mode number is zero, $m = 0$. The resultant time-dependent field components of the TM modes are:

$$B_r^{0,n,p}\left(r,\varphi,z,t\right) = 0\,,$$

$$
\begin{aligned}
B_{\varphi}^{0,n,p}\left(r,\varphi,z,t\right) &= -C\frac{j_{0,n}}{R}J_0^{'}\left(j_{0,n}\frac{r}{R}\right)\cos\left(p\pi\frac{z}{g}\right)\exp\left(\mathrm{i}\omega_{0,n,p}t\right)\,,\\
E_{r}^{0,n,p}\left(r,\varphi,z,t\right) &= -\mathrm{i}C\frac{p\pi}{g}\frac{c^2}{\omega_{0,n,p}}\frac{j_{0,n}}{R}J_0^{'}\left(j_{0,n}\frac{r}{R}\right)\sin\left(p\pi\frac{z}{g}\right)\exp\left(\mathrm{i}\omega_{0,n,p}t\right)\,,\\
E_{\varphi}^{0,n,p}\left(r,\varphi,z,t\right) &= 0,\\
E_{z}^{0,n,p}\left(r,\varphi,z,t\right) &= -\mathrm{i}C\frac{c^2}{\omega_{0,n,p}}\left(\frac{j_{0,n}}{R}\right)^2 J_0\left(j_{0,n}\frac{r}{R}\right)\cos\left(p\pi\frac{z}{g}\right)\exp\left(\mathrm{i}\omega_{0,n,p}t\right)\,,
\end{aligned}
\tag{43}
$$

employing a harmonic time dependence.

To calculate the loss parameters, we first need to compute the voltage drop per mode,

$$
V_{0,n,p} = \int_0^g E_z^{0,n,p}\left(r=0,z,t=\frac{z}{c}\right)\mathrm{d}z\,.
$$

Inserting $E_z^{0,n,p}$ and evaluating the integral yields:

$$
V_{0,n,p} = Cc\left(1-(-1)^p\exp\left(\frac{\mathrm{i}\omega_{0,n,p}g}{c}\right)\right)\,. \tag{44}
$$

We also need to know about the energy stored in each mode,

$$
U_{n,p} = \frac{1}{2\mu_0}\int_0^R\int_0^{2\pi}\int_0^g r\left(B_{\varphi}^{0,n,p}\right)\left(B_{\varphi}^{0,n,p}\right)^*\mathrm{d}z\mathrm{d}\varphi\mathrm{d}r\,,
$$

which is equivalent to Eq. (16), since $\frac{\epsilon_0}{2}\int\left|\mathbf{E}_n\left(\mathbf{r}\right)\right|^2\mathrm{d}^3r = \frac{1}{2\mu_0}\int\left|\mathbf{B}_n\left(\mathbf{r}\right)\right|^2\mathrm{d}^3r$. We use B_φ from Eq. (43) and solve the integral to get

$$
U_{0,n,p} = C^2\frac{j_{0,n}^2\pi g}{4}J_1^2\left(j_{0,n}\right)\left(1+\delta_{0,p}\right)\,. \tag{45}
$$

Here, we made use of the properties of the Bessel function to substitute $J_0^{'}\left(x\right) = -J_1\left(x\right)$, and introduced the Kronecker symbol, $\delta_{0,p}$, i.e., $\delta_{0,p} = 1$ if $p = 0$ and $\delta_{0,p} = 0$ otherwise.

With this, the loss parameters can be calculated via Eq. (18). For the cylindrical cavity, the loss parameters of the monopole eigenmode identified by the radial and axial mode numbers n and p are:

$$
k_{0,n,p} = \frac{1}{\pi\epsilon_0 g}\frac{2}{1+\delta_{0,p}}\frac{1-(-1)^p\cos\left(\frac{\omega_{0,n,p}g}{c}\right)}{j_{0,n}^2J_1^2\left(j_{0,n}\right)}\,. \tag{46}
$$

Figure 9 demonstrates the loss parameters of eigenmodes inside the given cylindrical cavity. The modes are first distinguished by their radial mode number n and then plotted against their axial mode number p. The graph shows that the loss parameters, and therefore the contribution strength of each mode to the wake potential, strongly vary. The mode with the strongest contribution is the $\mathrm{TM}_{0,1,1}$-mode, visible in the sharp peak displayed in the graph. It can be generally assumed that if we were to increase n even further, the contributions of the modes (the so-called *higher order modes*) would further decrease.

From the loss parameters, the wake function can be calculated similarly to Eq. (19),

$$
W_{||,0}\left(s\right) = \sum_{n=1}^{\infty}\sum_{p=0}^{\infty}2k_{0,n,p}\cos\left(\frac{\omega_{0,n,p}s}{c}\right)\,. \tag{47}
$$

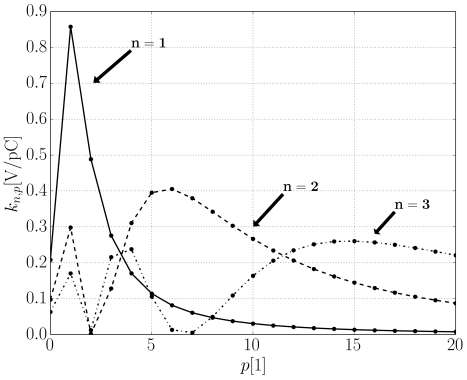

Fig. 9: Loss parameters of different monopole modes, discriminated by their radial mode number n and plotted against their axial mode number p. It is clearly visible that the strengths of the loss parameters, and thus their contributions to the wake potential, vary. The $\mathrm{TM}_{0,1,1}$ mode shows the strongest contribution of the displayed modes.

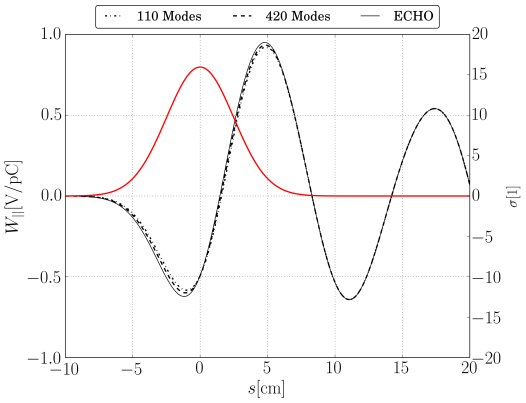

Fig. 10: Wake potential of a Gaussian pulse with $\sigma = 2.5\,\mathrm{cm}$ inside the exemplary pillbox cavity. The dash-dotted line denotes the analytical result for 110 considered modes; the dashed line for 420 modes. The solid line represents a numerical approximation of the wake potential computed with the software ECHO. All wake potentials are in very good agreement. The bunch shape function is plotted in red as a reference.

We now want to compute the wake potential of a Gaussian pulse. The bunch shape function of such a pulse is:

$$\psi(s) = \frac{1}{\sqrt{2\pi\sigma^2}} \exp\left(-\frac{s - s_0}{2\sigma^2}\right) . \tag{48}$$

Here, we assume that the Gaussian is centred on $s_0 = 0$, and that the width is $\sigma = 2.5\,\mathrm{cm}$. We will test the accuracy of the expansion for two different numbers of expansion functions, 110 (i.e., $1 \leq n \leq 10$ and $0 \leq p \leq 10$) and 420 modes (i.e., $1 \leq n \leq 20$ and $0 \leq p \leq 20$). The analytical results are compared with a numerical result obtained using the software ECHO [7]; the comparison is shown in Fig. 10. The results are in very good agreement; the difference in the accuracy of the analytical wake potentials is very small. From this, we can conclude that the influence of the higher-order modes on the wake potential is, indeed, comparatively small in this case, though still necessary to increase the accuracy of the analytical approximation of the wake potential.

5 The effects of wakefields

5.1 Ultra-relativistic wakefields

As described before, wakefields that remain in cavities can have large effects on trailing particles and bunches. Effectively, they represent *energy modulations* of the trailing particles—which can already hold true for particles of the same bunch as the wakefield-generating particle. Generally, this phenomenon is hardly predictable in complicated structures. These energy modulations can lead to an increase the emittance of the particle bunch. Usually, this is unwanted since—as soon as the beam has reached its design parameters—it might lead to beam instabilities if no measures are undertaken.

Nevertheless, there are certain cases in which the energy modulating effect of wake potentials can be useful. Devices called *wakefield dechirpers* or *wakefield silencers* are simple, passive accelerator components that are used to counteract the energy spreads of particle beams. Figure 11 compares the effect of a wakefield on a beam with a strong energy spread with that on a beam with no energy spread. In both cases, the modulation of the dechirper is represented by a linear energy gradient over

the coordinate s (red line). One beam has a low initial energy spread (dashed line), and so, adding the modulation of the wake potential, the resulting energy width after the wakefield is larger. The second beam, however, has a strong initial energy spread opposing the modulation of the dechirper (solid line). Here, applying the wake potential will effectively *lower* the total energy spread. This effect is currently studied at accelerators all over the world. Section 6 describes the wake potentials in a suitable structure in more detail.

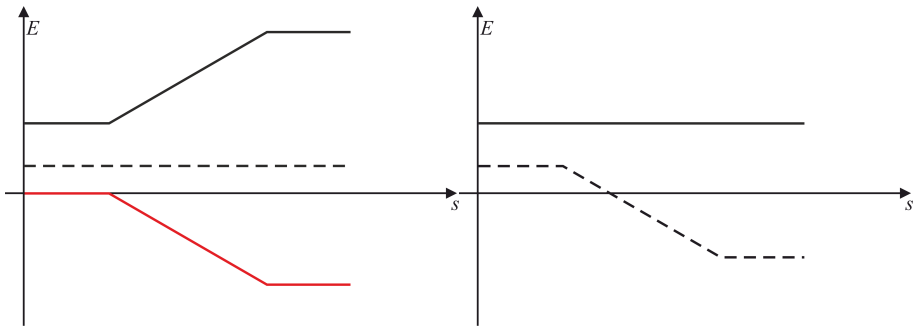

Fig. 11: The energy modulation induced by a wakefield (red) acts on two different beams, one with initial energy spread that is opposed to the modulation (black, solid line), one without (black, dashed line). Effectively, the modulation is added to the phase space of the beams, so that, after the dechirper, the energy width of the initially unchirped beam is *increased*, while the energy width of the chirped beam is *reduced*, owing to the interaction with the wake potential.

5.2 Space charge wakefields

So far, we have only dealt with ultra-relativistic wakefields, which are limited to the case $v \simeq c$. For $v < c$, space charge effects also play a role.

The reason for space charge effects are the Coulomb interactions of the charged particles, which play a role for non-ultra-relativistic beams and need to be taken into account there for every type of simulation or analytical consideration. Usually, these effects have an even larger influence on the trailing particles than the wakefields themselves. The effects of space charges can include the deflection of charged particles, the causing of beam instabilities, the generation of high (unwanted) field intensities, which in turn can lead to material breakdown, etc.

However, space charge effects are not the subject of these considerations. Thus, the reader is referred to Refs. [8] or [9] for more information.

6 Example 2: rectangular waveguide with dielectric linings

6.1 The eigenmodes

Figure 12 shows a rectangular waveguide with dielectric linings, which can be used as a wakefield dechirper ([10], [11]). The outer waveguide is made of a highly conductive material, e.g., copper or aluminium. As discussed before, the phase velocity of electromagnetic waves is smaller in the dielectric regions, which effectively slows down the image fields responsible for wake potentials, so that they can act on trailing particles as well. For this section, we will assume an exemplary waveguide with the parameters $a = 5\,\mathrm{cm}$, $b = 1.3\,\mathrm{cm}$, $L = 30\,\mathrm{cm}$; and dielectric coatings of a thickness $b - d = 1.5\,\mathrm{mm}$ and a relative permittivity, $\epsilon_\mathrm{r} = 4.8$.

As for the pillbox cavity considered before, the wake function is now analysed. First, it is required to take a look at the eigenmodes of these structures. We will consider three-dimensional eigenmodes here. In reality, this would be equivalent to the examination of a structure that is closed in all three

dimensions. This is of course unrealistic—for the dechirper to work, it must be passed by a particle beam, and consequently, the structure needs to be *open* in the z-direction. In this special case, however, owing to the properties of the structure, the wake function resulting from the three-dimensional eigenmodes of the close structure is identical to the wake function of the open structure.

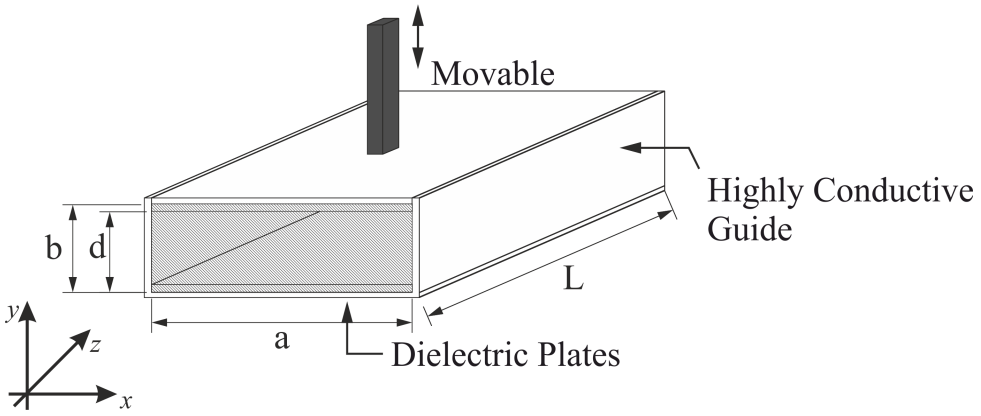

Fig. 12: A rectangular waveguide lined with two dielectric plates (shaded), which can be used as a dechirper. The outer waveguide is made of a highly conductive material. One or both plates (only the upper plate in the case shown) can be left unconnected to the remaining waveguide, so that the distance between the dielectrics can be adjusted.

The similarities between this dielectrically lined waveguide and an empty rectangular waveguide without dielectrics become obvious when the structure is considered for the first time. It would make sense if the eigenmodes reflect these similarities, i.e., if the eigenmodes are similar to TE and TM modes, which are the eigenmodes of conventional empty rectangular waveguides. Indeed, the eigenmodes of the lined waveguide are related to TE and TM modes and can be viewed as a superposition of them. This new set of eigenmodes, however, needs to reflect the dielectrics, which can be effectively described as a change in permittivity in one direction (the y-direction in this case). As a consequence, none of the longitudinal components of the eigenmodes' electric or magnetic fields is zero, as in the case of TE and TM modes but one of the *transverse* components is (the y-component, in this case). These kinds of mode are called *longitudinal-section electric (LSE)* modes (where $E_y = 0$) and *longitudinal-section magnetic (LSM)* modes (where $B_y = 0$) [6].

Their electric and magnetic fields can be derived from Maxwell's equations (assuming a harmonic time dependence and $\rho = 0, \mathbf{J} = \mathbf{0}$). However, the changing relative permittivity ϵ_r must be taken into account, so that:

$$\nabla \cdot \mathbf{D}\left(\mathbf{r}\right) = \epsilon_0 \nabla \cdot \left(\epsilon_\mathrm{r}(y)\mathbf{E}\left(\mathbf{r}\right)\right) = 0\,, \tag{49}$$

$$\nabla \cdot \mathbf{B}\left(\mathbf{r}\right) = 0\,, \tag{50}$$

$$\nabla \times \mathbf{E}\left(\mathbf{r}\right) = -\mathrm{i}\omega \mathbf{B}\left(\mathbf{r}\right)\,, \tag{51}$$

$$\nabla \times \mathbf{B}\left(\mathbf{r}\right) = \mathrm{i}\frac{\omega}{c_0^2}\epsilon_\mathrm{r}(y)\mathbf{E}\left(\mathbf{r}\right)\,. \tag{52}$$

Under the given circumstances, solution of these equations is analytically possible. In the x- and z-directions, the solution procedure follows a similar line as the derivation of the eigenmodes in an empty waveguide, since the phase velocity is the same everywhere in these directions. In the y- direction, the changing permittivity makes a straightforward solution like this impossible, though. To obtain an analytical expression for the eigenmodes, a Fourier expansion can be used to describe the unknown behaviour in the y- direction. Reference [6] provides a detailed example of the solution procedure for

the case of only one dielectric lining. The resulting electric fields (for two dielectric slabs) are

$$\mathbf{E}_{\mathrm{LSE}}\left(\mathbf{r}\right) = \omega_{\mathrm{LSE}} \begin{pmatrix} k_z \cos(k_x x) \sum\limits_{m=1}^{N} b_m \sin(k_{ym} y) \sin(k_z z) \\ 0 \\ -k_x \sin(k_x x) \sum\limits_{m=1}^{N} b_m \sin(k_{ym} y) \cos(k_z z) \end{pmatrix} ,$$

for LSE modes and

$$\mathbf{E}_{\mathrm{LSE}}\left(\mathbf{r}\right) = \frac{1}{\varepsilon_r(y)} \begin{pmatrix} -k_x \cos(k_x x) \sum\limits_{m=0}^{N} b_m k_{ym} \sin(k_{ym} y) \sin(k_z z) \\ \left(k_x^2 + k_z^2\right) \sin(k_x x) \sum\limits_{m=0}^{N} b_m \cos(k_{ym} y) \sin(k_z z) \\ -k_z \sin(k_x x) \sum\limits_{m=0}^{N} b_m k_{ym} \sin(k_{ym} y) \cos(k_z z) \end{pmatrix} ,$$

for LSM modes. Here, k_x, k_{ym}, and k_z represent the eigenvalues in the x-, y-, and z- directions. Just as in the case of the empty rectangular waveguide, all eigenvalues indicate the number of nodes or antinodes of the sine and cosine functions in the fields, e.g., $k_x = n\pi/a$, with a being the structure's width. Consequently, $k_{ym} = m\pi/b$ and $k_z = l\pi/L$, with b being the structure's height and L the structure's length. The index m *also* indicates the Fourier expansion; the expansion coefficients are q_m. Note that the summation is ceased after N terms, which makes the analytical expression an approximation of the real result. N is usually determined in a convergence study.

6.2 The electric field and longitudinal wake potential

As a next step, we want to determine the longitudinal wake potential inside a dielectrically lined rectangular waveguide. To achieve this, we first compute the wake function, and subsequently the loss parameters.

Until this point, we have determined the loss parameters using a relation between the stored energy and voltage drop per mode. This time, we want to calculate the wake function by a straightforward integration over the electric field. We still expand the electric field into a series of eigenmodes as shown in Eq. (15). We carry out this summation over both LSE and LSM modes. The time-dependent expansion coefficients are determined by solving Maxwell's equations for a point charge moving along the beam axis in the z-direction:

$$\nabla \cdot \mathbf{D}\left(\mathbf{r}\right) = \varepsilon_0 \nabla \cdot \left(\varepsilon_r(y)\mathbf{E}\left(\mathbf{r}\right)\right) = \rho\left(\mathbf{r}\right) , \tag{53}$$

$$\nabla \cdot \mathbf{B}\left(\mathbf{r}\right) = 0 , \tag{54}$$

$$\nabla \times \mathbf{E}\left(\mathbf{r}\right) = -\frac{\partial}{\partial t}\mathbf{B}\left(\mathbf{r}\right) , \tag{55}$$

$$\nabla \times \mathbf{B}\left(\mathbf{r}\right) = \mu_0 \mathbf{j}\left(\mathbf{r}\right) + \mu_0 \varepsilon_r(y) \varepsilon_0 \frac{\partial}{\partial t}\mathbf{E}\left(\mathbf{r}\right) . \tag{56}$$

The beam axis goes straight through the centre of the waveguide, so through the point $(x_{\mathrm{beam}}, y_{\mathrm{beam}}) = (a/2, b/2)$.

Once the coefficients have been determined, the longitudinal component of the electric field on the beam axis is integrated following Eq. (5). The process of the integration is tedious but analytically possible. We want to skip it here; Ref. [12] provides a more detailed solution of the wake function integral.

Within the scope of this paper, it is sufficient to discuss the final result of the integration. The integration automatically leads to a description of the wake function similar to Eq. (19). The cosine

dependence is a direct result of the integration; the summation is a remnant of the eigenmode expansion of the electric field. From this direct integration, the loss parameters can be read out as:

$$K_{n,m,l,\mathrm{LSE}} = -\frac{4}{\varepsilon_0 aL}\frac{k_x^2 k_z^2}{k_x^2+k_z^2}\left(\sum_{\text{even } m} q_m \sin\left(\frac{m\pi}{2}\right)\right)^2 \frac{\left(2-2\mathrm{e}^{\mathrm{i}l\pi}\cos\left(k_{0,\lambda}L\right)\right)}{\left(k_{0,\lambda}^2-k_z^2\right)^2},$$

$$K_{n,m,l,\mathrm{LSM}} = -\frac{4}{\varepsilon_0 aL}\frac{k_z^4}{k_{0,\mu}\left(k_x^2+k_z^2\right)}\left(\sum_{\text{even}m} q_m k_{y,m} \sin\left(\frac{m\pi}{2}\right)\right)^2 \frac{\left(2-2\mathrm{e}^{\mathrm{i}l\pi}\cos\left(k_{0,\mu}L\right)\right)}{\left(k_{0,\mu}^2-k_z^2\right)^2}.$$

To avoid confusing the loss parameters with the eigenvalues, we refer to them as $K_{n,m,l}$ in this case. The expressions of the loss parameters *appear* very lengthy and complicated; on a closer inspection, however, we see that they only depend on the mode characteristics and geometrical properties of the structure and thus can be determined without previous knowledge of the electric field. The electric field expansion is merely an intermediate analytical step to determine the formula for the loss parameters *once*. After this is done, it does not have to be repeated for every structure; rather the expressions for the loss parameters can be used straight from the formula at hand.

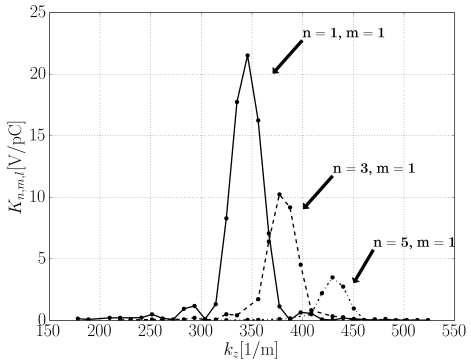

Fig. 13: Loss parameters of LSM modes with different n and m plotted over their longitudinal eigenvalue k_z. It can be seen that several modes exhibit much higher loss parameters than others, resulting in the observed peak structure.

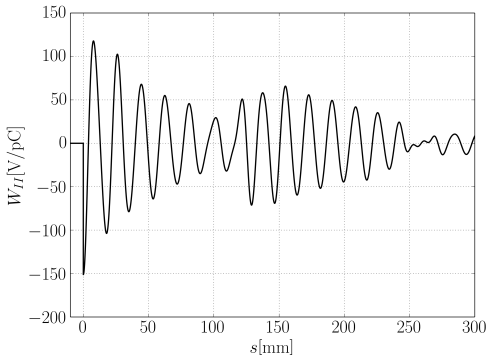

Fig. 14: Wake function in the exemplary dielectrically lined rectangular waveguide.

In Fig. 13, the loss parameters (of LSM modes of an arbitrary rectangular waveguide with an arbitrary dielectric lining) are again sorted (according to the numbers of nodes or antinodes in the transverse direction, n and m) and plotted against their longitudinal eigenvalue. As in the exemplary cylindrical cavity in Fig. 9, we observe several distinguished peaks. These eigenmodes obviously have the largest contribution to the wake function, while the loss parameters of other modes can be so small that their contributions to the wake function are negligible.

Following Eq. (19), the wake function can be calculated from the loss parameters. The wake function resulting from the modes displayed in Fig. 13 is displayed in Fig. 14.

At this point, we want to have a closer look at the influence of the bunch shape function on the resulting wake potential. According to Eq. (20), all that is needed to obtain the wake potential from the wake function is a convolution with the bunch shape function. This can be carried out easily, either numerically or analytically.

Figure 15 compares the short range wake potentials (i.e., the wake potentials in the vicinity of the bunch) of a Gaussian bunch (cf. Eq. (48)) and a so-called flat top pulse, i.e., a pulse with a constant

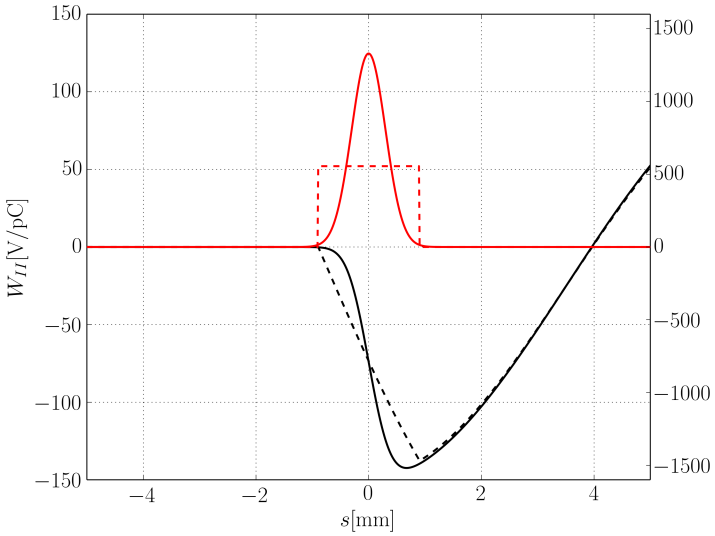

Fig. 15: Wake potentials of a Gaussian pulse (solid line, $\sigma = 0.3\,\mathrm{mm}$) and a flat top pulse (dashed line, pulse length $1.8\,\mathrm{mm}$) inside the exemplary rectangular waveguide with dielectric linings. The bunch shape functions are displayed in red for comparison.

particle distribution over the bunch length. Both bunches are designed to have the same length and both bunch shape functions are normalized to 1. It can be seen that the wake potentials over both bunch shapes refer to an overall energy loss. The maximum loss over the bunch shape is similar in both cases. This results from the normalization of the pulses: the convolution can generally be imagined as 'moving' the bunch shape function over the wake function and measuring the area enclosed by both. If the area under both used bunches is the same, owing to the normalization, it follows that the maximum energy loss should be nearly equal for both bunches. The gradient of the energy loss, however, shows significant differences when comparing both bunch shapes. The gradient for the flat top pulse is perfectly linear with sharp edges, while the gradient for the Gaussian pulse is steeper in the middle section and shows softened edges. This is a direct result of the different bunch shapes: the gradient for the flat top pulse is linear because of the equal distribution of particles over the bunch length and the gradient for the Gaussian pulse shows softened edges, owing to the Gaussian pulse's smooth behaviour.

For the total *energy loss* due to the wake potential, the bunch shape thus plays only a minor role, i.e., Fig. 15 clearly shows that the maximum energy loss over the particle bunch is nearly identical, and only dependent on the normalization of the bunch shape function (which should be 1 in any case). For the *phase space* of the bunch, however, the bunch shape function can have a significant influence. Here, it plays a role in determining 'how many' particles are subjected to a certain energy reduction. The dechirper can significantly alter the phase space of the bunch, depending on its bunch shape.

7 Summary and conclusions

In this paper, we introduced the basic quantities that are necessary to understand the concept of wakefields. We discussed the basic structural requirements for the generation of wakefields. We derived the longitudinal and transverse wake potential from the Lorentz force and introduced the Panofsky–Wenzel theorem, which links both quantities to each other. In addition, we briefly discussed the impedance as the Fourier transform of the wake potential.

When the eigenmodes of a structure are known, it is possible to derive the wake function, the wakefield of a point charge as a sum over each eigenmode's contribution. These contributions are called

loss factors. The wake function then serves as the Green's function for the calculation of the wake potential of an arbitrary bunch shape, and the total loss factor can give an insight into the total power loss due to the wakefield.

The effects of wakefields represent energy modulations, which consequently result in a modulation of the longitudinal and possibly also transverse phase space of a particle bunch. This is why wakefields, at least most of the time, are considered unwanted effects that have to be taken into consideration during the design process of accelerators, to mitigate their negative influence on the functionality of the accelerator. However, special structures called 'wakefield dechirper' can be used to utilize the energy modulating effect of wakefields to reduce the energy spread of particle beams.

Further reading

As complementary further reading, the following article for beginners on the topic might be helpful: P. Tenenbaum, *Fields in Waveguides—A Guide for Pedestrians*, 2003, available at `http://www.desy.de/~njwalker/uspas/coursemat/notes/unit_2_notes.pdf`.

References

[1] CST, *STUDIO SUITE®*, CST AG, Darmstadt, Germany.

[2] T. Weiland and R. Wanzenberg, *Wake Fields and Impedances* 100 (Springer, Berlin, 1992) p. 39. https://doi.org/10.1007/3-540-55250-226

[3] U. van Rienen, *Numerical Methods in Computational Electrodynamics: Linear Systems in Practical Applications* 12 (Springer, Berlin, 2001). https://doi.org/10.1007/978-3-642-56802-2

[4] P.B. Wilson, Introduction to wakefields and wake potentials, SLAC-PUB 4547 (1989).

[5] T.P. Wangler, *RF Linear Accelerators* (Wiley, Weinheim, 2008). https://doi.org/10.1002/9783527623426

[6] R.E. Collin, *Field Theory of Guided Waves* (IEEE Press, New York, 1991).

[7] I. Zagorodnov and T. Weiland, TE/TM field solver for particle beam simulations without numerical Cherenkov radiation, PRST-AB 8 (2005).

[8] A. Chao, *Physics of Collective Beam Instabilities in High Energy Accelerators* (Wiley, New York, 1993).

[9] D.A. Edwards and M.J. Syphers, *An Introduction to the Physics of High Energy Accelerators* (Wiley, New York, 1993). https://doi.org/10.1002/9783527617272

[10] F. Reimann et al., *A dielectrically lined rectangular waveguide as a wakefield dechirper for ELBE*, In G. Addamo et al. *Proc. of ICEAA 2015*, Torino, Italy, 2015, pp. 827, `http://ieeexplore.ieee.org/stamp/stamp.jsp?tp=&arnumber=7297229`.

[11] S. Antipov et al., *Passive Momentum Spread Compensation by a 'Wakefield Silencer'*, In J. Corbett et al. *Proc. of IPAC 2012*, New Orleans, USA, 2012, pp.598, `http://accelconf.web.cern.ch/accelconf/ipac2012/papers/moppp013.pdf` .

[12] K.L.F. Bane *et al.*, Wakefields and wakefield acceleration, SLAC-Pub. 3528 (1984).